

In-plane spin excitation of skyrmion bags

Shuang Li(李爽), Ke-Xin Li(李可欣), Zhao-Hua Liu(刘照华), Qi-Yuan Zhu(朱起源), Chen-Bo Zhao(赵晨博), Hu Zhang(张虎), Xing-Qiang Shi(石兴强), Jiang-Long Wang(王江龙), Rui-Ning Wang(王瑞宁), Ru-Qian Lian(连如乾), Peng-Lai Gong(巩朋来), and Chen-Dong Jin(金晨东)
Citation: Chin. Phys. B, 2023, 32 (**11**): 117503. DOI: 10.1088/1674-1056/acd327
Journal homepage: http://cpb.iphy.ac.cn; http://iopscience.iop.org/cpb

What follows is a list of articles you may be interested in

Magnonic band-pass and band-stop filters with structurally modulated waveguides

Lai-He Feng(冯来和), Mang-Yuan Ma(马莽原), Zhi-Hua Liu(刘智华), Kai-Le Xie(解凯乐), and Fu-Sheng Ma(马付胜)
Chin. Phys. B, 2023, 32 (**6**): 067503. DOI: 10.1088/1674-1056/ac8afb

Gate-voltage control of alternating-current-driven skyrmion propagation in ferromagnetic nanotrack devices

Xin-Yi Cai(蔡心怡), Zhi-Hua Chen(陈志华), Hang-Xiao Yang(杨航霄), Xin-Yan He(何鑫岩), Zhen-Zhen Chen(陈珍珍), Ming-Min Zhu(朱明敏), Yang Qiu(邱阳), Guo-Liang Yu(郁国良), and Hao-Miao Zhou(周浩淼)
Chin. Phys. B, 2023, 32 (**6**): 067502. DOI: 10.1088/1674-1056/acb420

Micromagnetic study of magnetization reversal in inhomogeneous permanent magnets

Zhi Yang(杨质), Yuanyuan Chen(陈源源), Weiqiang Liu(刘卫强), Yuqing Li(李玉卿), Liying Cong(丛利颖), Qiong Wu(吴琼), Hongguo Zhang(张红国), Qingmei Lu(路清梅), Dongtao Zhang(张东涛), and Ming Yue(岳明)
Chin. Phys. B, 2023, 32 (**4**): 047504. DOI: 10.1088/1674-1056/ac9359

Discrete modulational instability and bright localized spin wave modes in easy-axis weak ferromagnetic spin chains involving the next-nearest-neighbor coupling

Jiayu Xie(谢家玉), Zhihao Deng(邓志豪), Xia Chang(昌霞), Bing Tang(唐炳)
Chin. Phys. B, 2019, 28 (**7**): 077501. DOI: 10.1088/1674-1056/28/7/077501

Shape-manipulated spin-wave eigenmodes of magnetic nanoelements

Zhang Guang-Fu (张光富), Li Zhi-Xiong (李志雄), Wang Xi-Guang (王希光), Nie Yao-Zhuang (聂耀庄), Guo Guang-Hua (郭光华)
Chin. Phys. B, 2015, 24 (**9**): 097503. DOI: 10.1088/1674-1056/24/9/097503

In-plane spin excitation of skyrmion bags

Shuang Li(李爽)[1], Ke-Xin Li(李可欣)[1], Zhao-Hua Liu(刘照华)[1], Qi-Yuan Zhu(朱起源)[2], Chen-Bo Zhao(赵晨博)[3], Hu Zhang(张虎)[1], Xing-Qiang Shi(石兴强)[1], Jiang-Long Wang(王江龙)[1], Rui-Ning Wang(王瑞宁)[1], Ru-Qian Lian(连如乾)[1], Peng-Lai Gong(巩朋来)[1], and Chen-Dong Jin(金晨东)[1,†]

[1] *Key Laboratory of Optic-Electronic Information and Materials of Hebei Province, Research Center for Computational Physics, College of Physics Science and Technology, Hebei University, Baoding* 071002, *China*

[2] *College of Mathematics and Physics, Chongqing University of Science and Technology, Chongqing* 401331, *China*

[3] *Department of Materials Science and Engineering, Lanzhou University of Technology, Lanzhou* 730050, *China*

(Received 24 February 2023; revised manuscript received 5 May 2023; accepted manuscript online 6 May 2023)

Skyrmion bags are spin structures with arbitrary topological charges, each of which is composed of a big skyrmion and several small skyrmions. In this work, by using an in-plane alternating current (AC) magnetic field, we investigate the spin-wave modes of skyrmion bags, which behave differently from the clockwise (CW) rotation mode and the counterclockwise (CCW) rotation mode of skyrmions because of their complex spin topological structures. The in-plane excitation power spectral density shows that each skyrmion bag possesses four resonance frequencies. By further studying the spin dynamics of a skyrmion bag at each resonance frequency, the four spin-wave modes, i.e., a CCW-CW mode, two CW-breathing modes with different resonance strengths, and an inner CCW mode, appear as a composition mode of outer skyrmion–inner skyrmions. Our results are helpful in understanding the in-plane spin excitation of skyrmion bags, which may contribute to the characterization and detection of skyrmion bags, as well as the applications in logic devices.

Keywords: skyrmion bags, spin-wave mode, power spectral density, micromagnetic simulation

PACS: 75.75.–c, 75.75.Jn, 75.78.Cd, 12.39.Dc **DOI:** 10.1088/1674-1056/acd327

1. Introduction

Magnetic skyrmions, as topologically protected spin structures characterized by topological charges, have been widely studied in recent years.[1–17] Skyrmions have the characteristics of small size, topological protection, and low drive current density, which are conducive to the technical applications in high-density data storage equipment and low-energy-consumption spintronic devices.[18–22] In particular, the theoretical application of skyrmions has been extended to antiferromagnetic skyrmions, including racetrack memories, logic devices, spin nano-oscillators, and other promising spintronic devices derived from no spin Hall effect, zero stray field, and ultra-fast magnetization dynamics.[23–25] Recently, the interaction between spin wave and skyrmion has attracted considerable attention.[26–35] The propagating spin wave strongly depends on the excitation mode of a skyrmion in frequency, decay length, and group velocity.[33] The spin excitation of microwave AC magnetic field has attracted a lot of attention due to its potential application in the design of spin-wave devices.[27,35–41] As is well known, the spin-wave mode of skyrmion contains in-plane counterclockwise (CCW) rotation mode and clockwise (CW) rotation mode, and one out-of-plane breathing mode.[27,36] In addition, the spin-wave modes of 2π skyrmion,[37,38] elliptical skyrmion,[41] bimeron,[42] magnetic hopfion of three-dimensional (3D) space,[39] and 3D skyrmions lattice[43] have been studied. For example, the spin-wave mode of 2π skyrmions contains four in-plane modes including two CW modes, two CCW rotation modes, and two out-of-plane breathing modes;[37,38] the simple breathing mode of elliptical skyrmion splits into two complex breathing modes owing to the breaking of the rotational symmetry of the spin texture;[41] the spin-wave mode of bimeron presents an anisotropic property when the microwave magnetic field is applied in the plane;[42] the spin-wave mode of magnetic hopfion contains five modes of breathing and rotating characters;[39] the spin-wave mode of the 3D skyrmion lattice exhibits the CCW mode and CW mode that are excited in pair as the film thickness increases in the in-plane;[43] three coupled excitation modes were found in the antiferromagnetic exchange coupling disk.[44]

Skyrmion bags are spin structures with arbitrary topological charges, each of which is composed of several small skyrmions with opposite topological charges inside a larger skyrmion.[45–48] Compared with skyrmions, skyrmion bags have high topological charges to represent more information.[49,50] Skyrmion bags were discovered in the liquid crystal and the thin plate of B20 chiral FeGe magnet by polarized optical microscopy and Lorentz transmission electron microscopy, respectively.[46,51,52] By numerical simulations, the interaction of stable skyrmion bags in the liquid crystal is similar to that of large skyrmions.[46] Moreover,

†Corresponding author. E-mail: jinchd@hbu.edu

© 2023 Chinese Physical Society and IOP Publishing Ltd

the stability and current-induced motions of skyrmion bags have been investigated by micromagnetic simulations and in experiment,[46,48,51,53–55] the spintronic devices with tunable magnetic fields and variable topological charge driven by current have important application prospects.[46,48,51,53,54,56] Up to now, the in-plane spin excitation modes of skyrmion bags are still unclear. The in-plane spin excitations of skyrmion bags should be richer than those of skyrmions, because of the nested structure. Therefore, to manipulate skyrmion bags and promote the development of their potential applications, it is particularly important to study the spin excitation of skyrmion bags by applying an in-plane microwave magnetic field. In this work, we first calculate the ground state of the skyrmion bags, including the total topological charge and the total energy. Then, we calculate the power spectrum of the skyrmion bags and the corresponding spin-wave mode. Finally, we study the time evolution of skyrmion bag excitation, which contributes to a better understanding of each spin-wave mode.

2. Micromagnetic simulation details

The ground state and spin-wave resonance modes of skyrmion bags are obtained by solving the Landau–Lifshitz–Gilbert (LLG) equation with object oriented micromagnetic framework (OOMMF).[57] The LLG equation can be expressed as follows:

$$\frac{\mathrm{d}\boldsymbol{m}}{\mathrm{d}t} = -\gamma \boldsymbol{m} \times \boldsymbol{H}_{\mathrm{eff}} + \alpha \boldsymbol{m} \times \frac{\mathrm{d}\boldsymbol{m}}{\mathrm{d}t}, \tag{1}$$

where $\boldsymbol{m}$ is the unit vector of magnetization, α is the Gilbert damping parameter and is set to 0.5 and 0.01 for the solution of the ground state and the resonant excitation procedure, respectively, $\boldsymbol{H}_{\mathrm{eff}}$ is the total effective field composed of the Heisenberg exchange field, the Dzyaloshinskii–Moriya interaction (DMI) field, the uniaxial anisotropy field, the demagnetization field, and the applied field. The applied field is set to $\boldsymbol{B}_x(t) = B_0 \mathrm{sinc}\,(2\pi f t)$ and $\boldsymbol{B}_x(t) = B_x \sin(2\pi f t)$ for the excitation spectrum solution and the time evolution solution, respectively. The simulation radius of the nanodisk is 100 nm and the cell size is 1 nm×1 nm×0.4 nm. Typical parameters for Co on heavy metal substrate parameters are cited from Refs. [21,54,58], exchange constant $A = 1.5 \times 10^{-11}$ J/m, DMI constant $D = 3.5 \times 10^3$ J/m^2, uniaxial anisotropy constant $K_{\mathrm{u}} = 0.8 \times 10^6$ J/m^3, and saturation magnetization $M_{\mathrm{s}} = 5.8 \times 10^5$ A/m. Such parameters guarantee the existence of different types of skyrmion bags, as reported in Refs. [40,53,54,59]. The ground state of skyrmion bag is denoted by S(n), where n represents the number of inner skyrmions. The definition of skyrmion bag in this work is similar to that in Ref. [46], so the skyrmion bag shown in Fig. 1(a) is denoted as S(4). Owing to the boundary potential and the large enough interfacial DMI, the initial position of the outer skyrmion (the polarity is +1) is stable in the middle of the nanodisk, and the four inner skyrmions (the polarity is −1) are centrally symmetric. The skyrmion bags are described by topological charge Q,[3,60]

$$Q = \frac{1}{4\pi} \iint q \mathrm{d}x\mathrm{d}y, \quad q = \boldsymbol{m} \cdot \left(\frac{\partial \boldsymbol{m}}{\partial x} \times \frac{\partial \boldsymbol{m}}{\partial y} \right), \tag{2}$$

where Q is the total topological charge. Figure 1(b) shows the topological density distribution corresponding to S(4). The topological density of the outer skyrmion boundary region reaches to 4.2×10^{15} m^{-2}, and the topological density of the four inner skyrmions' region has the lowest value of -2.44×10^{15} m^{-2}. By integrating the topological density of the entire nanodisk, the topological charge of S(4) is −3. It should be noted that if the background magnetization direction is reversed, then the topological charge sign of skyrmion bags will be reversed correspondingly.

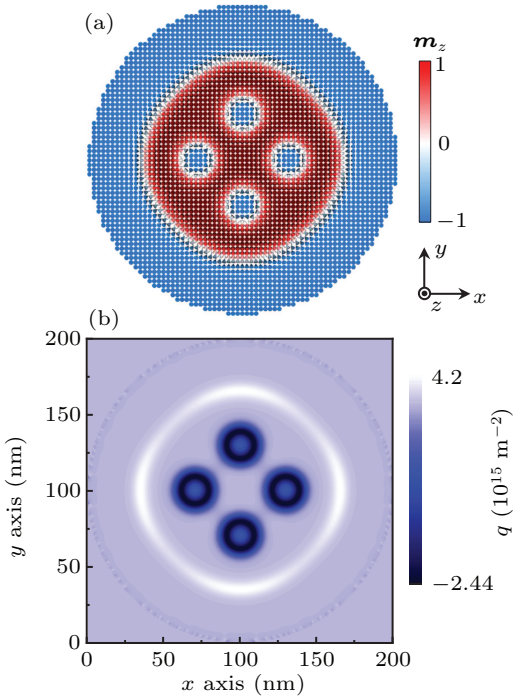


Fig. 1. (a) Ground state of S(4) skyrmion bag, with color map characterizing the direction of out-of-plane magnetization m_z, red color representing the magnetization orientation along the z direction, and blue color denoting that along the $-z$ direction. (b) Topological density of skyrmion bag, with total topology charge being −3 for S(4).

3. Results and discussion

3.1. Ground state, total topological charge and total energy of S(0)–S(9)

We first calculate the ground state of S(0)–S(9) in Fig. 2 by micromagnetic simulation. To obtain the ground state of skyrmion bag, we place a large bubble into the nanodisk and then set small bubbles into the large bubble. Then, we relax the magnetic system and obtain the minimum value of the total energy by using a conjugate gradient method implemented in the OOMMF code.[57] The magnetic system is considered stable when the change of the measured total energy is less than $1/10^5$ in 10 ns.[53] The arrows point in the z-direction

away from the center of the skyrmion, and an elementary full skyrmion (S(0)) has a topological charge -1 as shown in Fig. 2(a). Inside a stretched skyrmion, the arrows point in the $-z$ direction, and a skyrmion placed here has $Q+1$, so the 2π-skyrmion (S(1)) has a topological charge as shown in Fig. 2(b). Furthermore, as $n > 1$, S(n) represents different skyrmion bags shown in Figs. 2(c)–2(j), and their stabilities have been systematically analyzed in thin magnetic films by simulations.[53] The magnetic moment direction of the ground state of S(0)–S(9) are shown in Fig. 2. Skyrmion bag is a nested structure of small skyrmions contained by a big skyrmion, and its size becomes larger due to the increasing number of skyrmions. In addition, to further investigate the properties of skyrmion bag, we calculate the functional relationship between the total topological charge (Q) and S(n), and that between the total energy (E) and S(n).

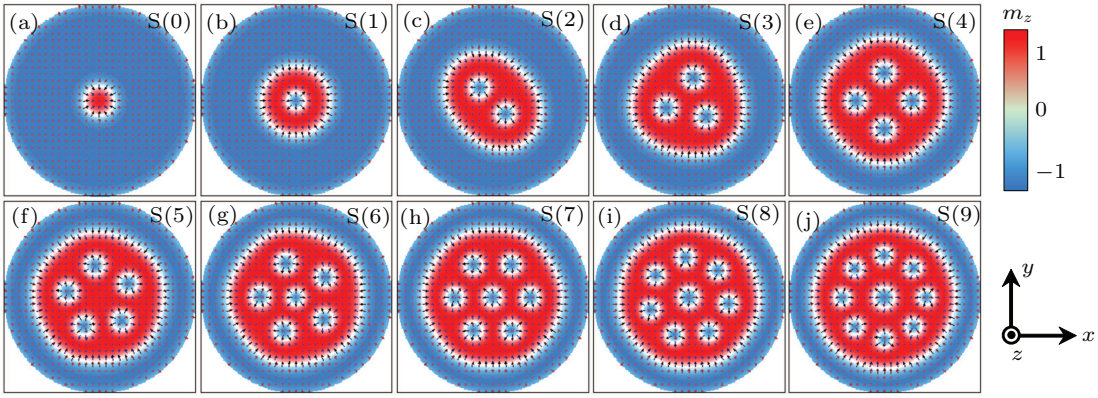


Fig. 2. Schematics of ground state of (a) simple skyrmion S(0), (b) 2π-skyrmion S(1), and ((c)–(j)) skyrmion bags S(2)–S(9) in circular nanodisk with a radius of 100 nm.

Figure 3(a) shows that Q decreases from 1 to 8 with n increasing from 0 to 9, so $Q = 1 - n$. Figure 3(b) shows that E increases from 2.448×10^{-18} J (S(0)) to 3.277×10^{-18} J (S(9)) with the increases of S(n), which means that the stability of the skyrmion bags decreases as the number of inner skyrmions increases.

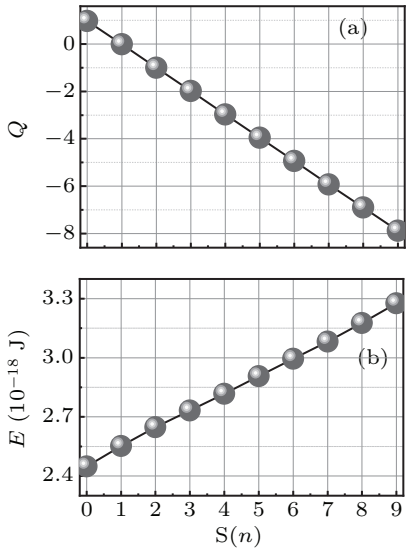


Fig. 3. The S(n)-dependent total topological charge Q (a) and total energy E (b) of the skyrmion bags.

3.2. Map of power spectral density of skyrmion bags

To investigate the spin excitation of skyrmion bags, the power spectral density (PSD) of skyrmion bag is calculated as shown in Fig. 4. Specifically, we study the map of PSD of skyrmion bags varying with n to compare the differences among the different modes of skyrmion bags. For the excitation spectrum of each skyrmion bag, the map of PSD indicates the number of resonance frequencies as well as the linewidth of each resonant frequency, the magnitude of the peak amplitude is represented by the color depth of the color code. The excitation pulse is the sinc function $\boldsymbol{B}_x(t) = B_0 \mathrm{sinc}(2\pi f t)$, where the amplitude B_0 is 10 mT in the x-axis direction as shown in Fig. 4(a). The cutoff frequency is set to 50 GHz. The excitation frequency can be obtained by the fast Fourier transform (FFT) of the oscillation of the in-plane x component of magnetization, and then the PSD phase diagram of skyrmion bags with S(n) is obtained by changing S(n) as shown in Fig. 4(b). In earlier work, for S(0) as a single skyrmion, the number of in-plane excitation modes depends on the DMI value;[41] the in-plane excitation mode of 2π skyrmion S(1) exhibits two resonance modes, and the relationship between the resonant mode and the uniform magnetic field is studied.[37] We mainly focus on the excitation spectrum of skyrmion bag, i.e., S(n) > 1, there are four in-plane resonance modes of skyrmion bags, which are different from those of skyrmions and 2π skyrmions. The resonance frequency of mode 1 increases monotonically with S(n) increasing from 0.7 GHz (S(2)) to 4.9 GHz (S(9)). With S(n) increasing from S(2) to S(9), the resonance frequency of mode 2 and mode 4 remain unchanged at 10 GHz and 45 GHz, respectively. The resonance frequency of mode 3 decreases from 16.3 GHz (S(1)) to 14.5 GHz (S(3)) and then increases to 22.9 GHz (S(9)). It is found that the number of modes of the

skyrmion bag does not change with n when $n > 2$, but the resonance frequencies of different modes shift with n. Because each skyrmion bag has four specific modes excited by the in-plane microwave magnetic field, these modes may be used for detecting and characterizing skyrmion bags.

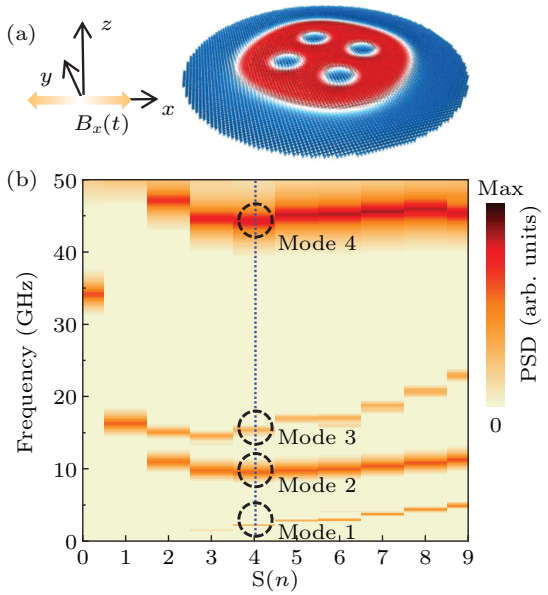


Fig. 4. Map of power spectral density of skyrmion bags. (a) Excitation pulse $\boldsymbol{B}_x(t) = B_0 \mathrm{sinc}(2\pi ft)$, where $B_0 = 10$ mT is applied to the nanodisk of ground state of S(n) along the x direction in the x–y plane, taking S(4) for example. (b) Resonance frequency of in-plane modes changing with S(n) increasing from S(0) to S(9). Take S(4) for example, each skyrmion bag has four main modes. The color code of the PSD indicates the peak amplitude of excitation spectrum, i.e., imaginary part of susceptibility (Imχ).

3.3. In-plane spin-wave modes of skyrmion bags

Taking the S(4)-type skyrmion bag for example, the spin-wave modes of skyrmion bags at in-plane resonance frequencies are studied in detail, as shown in Fig. 5, the four in-plane resonance frequencies of S(4) are 2.2 GHz, 9.6 GHz, 15.4 GHz, and 44.3 GHz, respectively. For mode 1 at 2.2 GHz, the resonance amplitude of δm_z in the in-plane magnetization region of the outer skyrmion and inner skyrmion are both larger. The phase of the spatial distribution of the outer skyrmion changes continuously from $-\pi$ to π, and the phase changes of the four inner skyrmions are opposite to that of the outer skyrmion. For mode 2 at 9.6 GHz, the spatial distribution of the resonance amplitude of the outer skyrmion is larger than those of four inner skyrmions. The phase of the outer skyrmion region changes continuously from π to $-\pi$, and the phase difference in phase among the four inner skyrmions is $\pi/2$. For mode 3 at 15.4 GHz, the resonance distribution and phase variation are similar to those for mode 2, and the difference is that the resonance amplitude of the inner skyrmions is larger than that of the outer skyrmion. For mode 4 at 44.3 GHz, the spatial distribution of the resonance amplitudes is concentrated in the region of the inner skyrmions, and the phases of the four inner skyrmions all vary from π to $-\pi$.

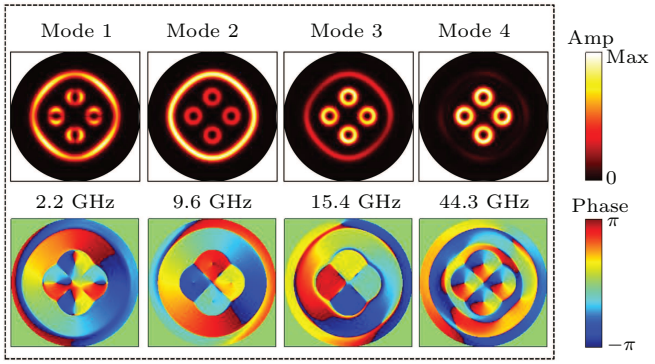


Fig. 5. Strong in-plane spin-wave modes of skyrmion bags, with the first row and second row showing FFT amplitude and phase of δm_z, respectively, and corresponding to the four modes marked in Fig. 4.

3.4. Compound modes of rotation and breathing of skyrmion bags under in-plane microwave magnetic field

To further identify each spin-wave mode shown in Fig. 5, we investigate the magnetization component of the skyrmion bags at different times by applying a sine-function magnetic fields with different resonance frequencies, to the bags as shown in Fig. 6. The sine-function microwave magnetic field is expressed as $\boldsymbol{B}_x(t) = B_x \sin(2\pi ft)$, where $B_x = 10$ mT, f is the resonance frequency of each spin-wave mode. To observe the changes of the skyrmion bag under the action of the sine-function microwave magnetic field, we present the snapshots of $\delta m_z(t)$ at different times, where $\delta m_z(t)$ is the difference between the z-direction magnetization component changing with time and the z-direction magnetization component of the initial state, and it can be expressed as $\delta m_z(t) = m_z(t) - m_z(0)$, where $\delta m_z(t)$ is normalized to observe its variation more clearly. The time evolution of the skyrmion bag in a circle is shown in five snapshots in Fig. 6(a) when an in-plane microwave AC magnetic field at 2.2 GHz is applied to the skyrmion bags. The outer skyrmion and the inner skyrmion exhibit the CCW rotation mode and the CW rotation mode, respectively. The opposite directions of the inner rotation and the outer rotation result from the opposite directions of the opposite polarity of the inner skyrmions and the outer skyrmion. The CW modes of the inner skyrmions are not seen to be in phase, resulting from the rotation symmetry of the inner skyrmions being broken due to the influence of the CCW mode of the outer skyrmion. Figure 6(b) shows the spin-wave modes at 9.6 GHz: the outer skyrmion shows the CW rotation mode, and the weak breathing mode of the inner skyrmions traces the CW rotation mode of the outer skyrmion. Figure 6(c) shows the spin-wave modes at 15.4 GHz, i.e., the weak CW rotation mode of the outer skyrmion and the strong breathing mode of the inner skyrmions following the CW rotation mode of the outer skyrmion. For the spin-wave modes at 9.6 GHz

and 15.4 GHz, the outer skyrmion shows the same CW rotation mode as a single skyrmion with the increase in frequency; the inner skyrmions do not show the CCW mode but a breathing mode following the CW mode of the outer skyrmion, because the rotation symmetry of the skyrmion bag is broken with the increase in frequency. The supplementary material video shows the time evolutions of m_z and δm_z at various resonance frequencies, which can conduce to the understanding of the in-plane spin-wave modes of skyrmion bags, where δm_z is normalized. As can be seen from videos 2 and 3, the inner skyrmion of mode 2 with the largest distance from the outer domain wall is always the largest; mode 3 is a similar mode, with the key difference being that the inner skyrmion with the largest distance from the outer domain wall is always the smallest. The higher frequency of mode 3 causes the breathing of inner skyrmions to fail to keep up with the rotation change of the outer skyrmion. Figure 6(d) shows the spin-wave modes of the skyrmion bag at 44.3 GHz, in which the outer skyrmion has almost no resonance, and the inner skyrmion shows a CCW rotation mode. It can be seen from video 4 that the CCW modes of the four inner skyrmions are in phase without the influence of the domain wall of the outer skyrmion.

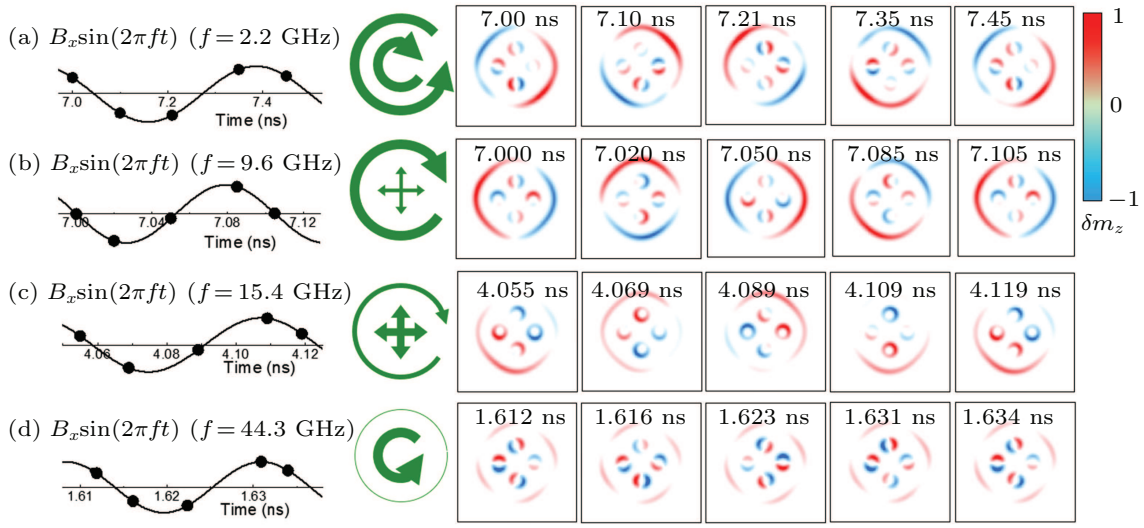


Fig. 6. Composite mode of rotation and respiration of skyrmion bags in in-plane microwave magnetic field. (a)–(d) Four microwave magnetic fields at different frequencies correspond to the four spin-wave modes in Fig. 5. The left side is for sine-function microwave magnetic field with different directions and frequencies applied, and on the right-hand side are time snapshots of the δm_z of the skyrmion bags excited by different sine-function microwave magnetic fields. The times of four snapshots under the sine-function microwave magnetic field are marked out in the sine function images on the left-hand side by the black solid circle, and in the middle is the manifestation of spin-wave mode.

The above results provide a method to manipulate the dynamics of skyrmion bags in nanostructures by using a microwave magnetic field. For example, in the future, it will be possible to create,[61] drive[62] or even detect and characterize the skyrmion bags[63] by using microwave magnetic fields, which is similar to the reported method of operating skyrmions. In addition, the in-plane spin-wave modes of skyrmion bags include some new rotation-breathing coupling modes (the breathing mode generally appears in the out-of-plane excitation of the skyrmion[40]), which can be used for realizing the logic devices and also contribute to the development of skyrmion bags-based oscillators.

4. Conclusions

In summary, we first investigated the ground state of skyrmion bag. We showed that the energy of geometrically confined skyrmion bags follows the same nearly linear dependence on topological charge as that of an extended system. By studying the in-plane excitation of skyrmion bags, we found that the skyrmion bags have four complex main spin-wave modes, which are different from the simple rotation modes of skyrmions. In addition, we focused our attention on the spin excitation of skyrmion bags. With the increase of resonance frequency, the four in-plane resonance modes are found as follows: for mode 1, the outer skyrmion is in a strong CCW rotation mode and each inner skyrmion is in a strong resonance CW rotation mode; for mode 2, the outer skyrmion is in a strong CW rotation mode and the inner skyrmions are of weak breathing mode; for mode 3, the outer skyrmion is in a weak CW rotation mode and inner skyrmions are of strong breathing mode; for mode 4, the outer skyrmion almost has no resonance and each inner skyrmion is in a strong CCW rotation mode. Because the skyrmion bags possess nested structures of skyrmions, they have some more complex in-plane spin-wave modes than a single skyrmion. Our results conduce to the understanding of the in-plane spin-wave modes of skyrmion bags and may provide a reference for designing the spintronic and logic devices.

Supplementary material

For more information about the micromagnetic simulation, readers may refer to the time domain variation videos of m_z and δm_z at each resonance frequency in the supplementary material, videos 1–4 corresponding to modes 1–4 in sequence.

Acknowledgements

Project supported by the National Natural Science Foundation of China (Grant Nos. 12104124 and 12274111), the Natural Science Foundation of Hebei Province, China (Grant Nos. A2021201001 and A2021201008), the Central Guidance Fund on the Local Science and Technology Development of Hebei Province, China (Grant No. 236Z0601G), the Post-graduate's Innovation Fund Project of Hebei Province, China (Grant No. CXZZSS2023007), the Advanced Talents Incubation Program of the Hebei University, China (Grant Nos. 521000981395, 521000981423, 521000981394, and 521000981390), the Research Foundation of Chongqing University of Science and technology, China (Grant No. ckrc2019017), and the High-Performance Computing Center of Hebei University, China.

References

[1] Roessler U K, Bogdanov A and Pfleiderer C 2006 *Nature* **442** 797
[2] Seki S, Yu X Z, Ishiwata S and Tokura Y 2012 *Science* **336** 198
[3] Nagaosa N and Tokura Y 2013 *Nat. Nanotechnol.* **8** 899
[4] Kim J V, Garcia-Sanchez F, Sampaio J, Moreau-Luchaire C, Cros V and Fert A 2014 *Phys. Rev. B* **90** 064410
[5] Zhou Y and Ezawa M 2014 *Nat. Commun.* **5** 4652
[6] Jiang W J, Upadhyaya P, Zhang W, Yu G, Jungfleisch M B, Fradin F Y, Pearson J E, Tserkovnyak Y, Wang K L, Heinonen O, te Velthuis S G E and Hoffmann A 2015 *Science* **349** 283
[7] Du H F, Che R C, Kong L Y, Zhao X B, Jin C M, Wang C, Yang J Y, Ning W, Li R W, Jin C Q, Chen X H, Zang J D, Zhang Y H and Tian M L 2015 *Nat. Commun.* **6** 8504
[8] Boulle O, Vogel J, Yang H, Pizzini S, de Souza Chaves D, Locatelli A, Menteş T O, Sala A, Buda-Prejbeanu L D, Klein O, Belmeguenai M, Roussigné Y, Stashkevich A, Chérif S M, Aballe L, Foerster M, Chshiev M, Auffret S, Miron I M and Gaudin G 2016 *Nat. Nanotechnol.* **11** 449
[9] Jin C D, Song C K, Wang J S, Xia H Y, Wang J B and Liu Q F 2017 *J. Appl. Phys.* **122** 223901
[10] Yang Y C, Liu T, Bi L and Deng L J 2021 *J. Alloys Compd.* **860** 158235
[11] Wang X R, Hu X C and Wu H T 2021 *Commun. Phys.* **4** 142
[12] Wu H T, Hu X C, Jing K Y and Wang X R 2021 *Commun. Phys.* **4** 210
[13] Ye C, Li L L, Shu Y, Li Q R, Xia J, Hou Z P, Zhou Y, Liu X X, Yang Y Y and Zhao G P 2022 *Rare Metals* **41** 2200
[14] Du H F and Wang X R 2022 *Chin. Phys. B* **31** 087507
[15] Ma Y X, Wang J N, Zeng Z Z, Yuan Y Y, Yang J X, Liu H B, Zhang S F, Wei J W, Wang J B, Jin C D and Liu Q F 2022 *J. Magn. Magn. Mater.* **564** 170061
[16] Jing D Y, Wang H Y, Guo W X and Liu W M 2023 *Chin. Phys. B* **32** 017401
[17] Lin T, Wang C X, Qiu Z Y, Chen C, Xing T, Sun L, Liang J H, Wu Y Z, Shi Z and Lei N 2023 *Chin. Phys. B* **32** 027505
[18] Chui C P and Zhou Y 2015 *AIP Adv.* **5** 097126
[19] Jin C D, Song C K, Wang J B and Liu Q F 2016 *Appl. Phys. Lett.* **109** 182404
[20] Luo S J, Zhang Y, Shen M K, Ou-Yang J, Yan B Q, Yang X F, Chen S, Zhu B P and You L 2017 *Appl. Phys. Lett.* **110** 112402
[21] Jin C D, Wang J B, Wang W W, Song C K, Wang J S, Xia H Y and Liu Q F 2018 *Phys. Rev. Appl.* **9** 044007
[22] Hirohata A, Yamada K, Nakatani Y, Prejbeanu I L, Dieny B, Pirro P and Hillebrands B 2020 *J. Magn. Magn. Mater.* **509** 166711
[23] Shen L C, Xia J, Zhao G P, Zhang X C, Ezawa M, Tretiakov O A, Liu X X and Zhou Y 2018 *Phys. Rev. B* **98** 134448
[24] Shen L C, Xia J, Zhao G P, Zhang X C, Ezawa M, Tretiakov O A, Liu X X and Zhou Y 2019 *Appl. Phys. Lett.* **114** 042402
[25] Liang X, Xia J, Zhang X C, Ezawa M, Tretiakov O A, Liu X X, Qiu L, Zhao G P and Zhou Y 2021 *Appl. Phys. Lett.* **119** 062403
[26] Petrova O and Tchernyshyov O 2011 *Phys. Rev. B* **84** 214433
[27] Mochizuki M 2012 *Phys. Rev. Lett.* **108** 017601
[28] Iwasaki J, Beekman A J and Nagaosa N 2014 *Phys. Rev. B* **89** 064412
[29] Zhang X C, Ezawa M, Xiao D, Zhao G P, Liu Y W and Zhou Y 2015 *Nanotechnology* **26** 225701
[30] Liu Y Z, Yin G, Zang J D, Shi J and Lake R K 2015 *Appl. Phys. Lett.* **107** 152411
[31] Zhang X C, Muller J, Xia J, Garst M, Liu X X and Zhou Y 2017 *New J. Phys.* **19** 065001
[32] Yokouchi T, Hoshino S, Kanazawa N, Kikkawa A, Morikawa D, Shibata K, Arima T, Taguchi Y, Kagawa F, Nagaosa N and Tokura Y 2018 *Sci. Adv.* **4** 8
[33] Seki S, Garst M, Waizner J, Takagi R, Khanh N D, Okamura Y, Kondou K, Kagawa F, Otani Y and Tokura Y 2020 *Nat. Commun.* **11** 256
[34] Zhang X C, Xia J, Tretiakov O A, Diep H T, Zhao G P, Yang J B, Zhou Y, Ezawa M and Liu X X 2021 *Phys. Rev. B* **104** L220406
[35] Chen J L, Yu H M and Gubbiotti G 2022 *J. Phys. D* **55** 123001
[36] Mruczkiewicz M, Krawczyk M and Guslienko K Y 2017 *Phys. Rev. B* **95** 094414
[37] Song C K, Ma Y X, Jin C D, Wang J S, Xia H Y, Wang J B and Liu Q F 2019 *New J. Phys.* **21** 083006
[38] Vigo-Cotrina H 2021 *J. Magn. Magn. Mater.* **537** 168166
[39] Bo L, Ji L Z, Hu C L, Zhao R Z, Li Y X, Zhang J and Zhang X F 2021 *Appl. Phys. Lett.* **119** 212408
[40] Zeng Z Z, Song C K, Wang J B and Liu Q F 2022 *J. Phys. D* **55** 185001
[41] Jin C D, Li S, Zhang H, Wang R N, Wang J L, Lian R Q, Gong P L and Shi X Q 2022 *New J. Phys.* **24** 043005
[42] Jin C D, Li S, Zhang H, Wang R N, Wang J L, Lian R Q, Gong P L and Shi X Q 2022 *New J. Phys.* **24** 073013
[43] Savchenko A S, Kuchkin V M, Rybakov F N, Blügel S and Kiselev N S 2022 *APL Mater.* **10** 071111
[44] Xing L D, Hua D Y and Wang W W 2018 *J. Appl. Phys.* **124** 123904
[45] Leonov A O and Pappas C 2019 *Phys. Rev. B* **99** 144410
[46] Foster D, Kind C, Ackerman P J, Tai J S B, Dennis M R and Smalyukh I I 2019 *Nat. Phys.* **15** 655
[47] Kuchkin V M, Barton-Singer B, Rybakov F N, Blugel S, Schroers B J and Kiselev N S 2020 *Phys. Rev. B* **102** 144422
[48] Zeng Z Z, Zhang C L, Jin C D, Wang J N, Song C K, Ma Y X, Liu Q F and Wang J B 2020 *Appl. Phys. Lett.* **117** 172404
[49] Finazzi M, Savoini M, Khorsand A R, Tsukamoto A, Itoh A, Duo L, Kirilyuk A, Rasing T and Ezawa M 2013 *Phys. Rev. Lett.* **110** 177205
[50] Zhang X C, Xia J, Zhou Y, Wang D W, Liu X X, Zhao W S and Ezawa M 2016 *Phys. Rev. B* **94** 094420
[51] Tang J, Wu Y D, Wang W W, Kong L Y, Lv B Y, Wei W S, Zang J D, Tian M L and Du H F 2021 *Nat. Nanotechnol.* **16** 1086
[52] Tang J, Wu Y D, Kong L Y, Wang W W, Chen Y T, Wang Y H, Soh Y, Xiong Y M, Tian M L and Du H F 2021 *Natl. Sci. Rev.* **8** 7
[53] Kind C, Friedemann S and Read D 2020 *Appl. Phys. Lett.* **116** 022413
[54] Kind C and Foster D 2021 *Phys. Rev. B* **103** L100413
[55] Kuchkin V M, Chichay K, Barton-Singer B, Rybakov F N, Blügel S, Schroers B J and Kiselev N S 2021 *Phys. Rev. B* **104** 165116
[56] Göbel B, Schäffer A F, Berakdar J, Mertig I and Parkin S S P 2019 *Sci. Rep.* **9** 12119
[57] Donahue M J and Porter D G http://math.nist.gov/oommf [2023-02-24]
[58] Sampaio J, Cros V, Rohart S, Thiaville A and Fert A 2013 *Nat. Nanotechnol.* **8** 839
[59] Xia J, Zhang X C, Ezawa M, Shao Q M, Liu X X and Zhou Y 2020 *Appl. Phys. Lett.* **116** 022407
[60] Moutafis C, Komineas S and Bland J A C 2009 *Phys. Rev. B* **79** 224429
[61] Li Z X, Chen Y F, Zhou Z W, Nie Y Z, Xia Q L, Wang D W and Guo G H 2017 *J. Magn. Magn. Mater.* **433** 216
[62] Ikka M, Takeuchi A and Mochizuki M 2018 *Phys. Rev. B* **98** 184428
[63] Okamura Y, Kagawa F, Mochizuki M, Kubota M, Seki S, Ishiwata S, Kawasaki M, Onose Y and Tokura Y 2013 *Nat. Commun.* **4** 2391